

# Numerical Simulations of the Combustion Process in a Research Thruster operating with $N_2O/C_2H_4$ and Comparison to Experimental Data

Lukas Werling<sup>\*†</sup>, Ansgar Bachmann<sup>\*</sup>, Nikolaos Perakis<sup>‡</sup>, Torsten Methling<sup>§</sup>, Corina Janzer<sup>§</sup>

<sup>\*</sup> German Aerospace Center (DLR), Institute of Space Propulsion  
Im Langen Grund D-74239 Hardthausen

<sup>‡</sup> Technical University of Munich  
Arcisstrasse 21 D-80333 Munich

<sup>§</sup> German Aerospace Center (DLR), Institute of Combustion Technology  
Pfaffenwaldring 38-40 D-70569 Stuttgart

Lukas.Werling@dlr.de · Ansgar.Bachmann@dlr.de · Nikolaos.Perakis@tum.de ·  
Torsten.Methling@dlr.de · Corina.Janzer@kit.edu

<sup>†</sup>Corresponding author

## Abstract

Since decades, the highly toxic hydrazine is used as propellant for in-space propulsion. During the last years, several non-toxic alternatives – so-called green propellants – were developed. One promising replacement for hydrazine are mono- and bipropellants consisting of nitrous oxide and one or more fuels. Here, the German Aerospace Center (DLR) investigates a propellant consisting of nitrous oxide and ethane in premixed monopropellant configuration. In parallel to experimental work performed at DLR's test site in Lampoldshausen, reaction mechanisms for the combustion of  $N_2O/C_2H_4$  and  $N_2O/C_2H_6$  were developed by DLR's Institute of Combustion Technology. To gain insight in the combustion processes, the reaction mechanisms were used to simulate the combustion inside a research thruster. For modelling, the commercial CFD solver Ansys Fluent was used. In sum two different basic configurations were simulated: 1) The reaction of premixed  $N_2O/C_2H_4$  by employing the  $N_2O/C_2H_4$  mechanisms and 2) the reaction of premixed  $N_2O/C_2H_4$  by using the  $N_2O/C_2H_6$  mechanisms. As for all cases a large experimental database is available, the results of the simulations were directly compared to the experimental results regarding chamber pressure, thrust and wall heat flux. To match the experimental data, different reaction and turbulence models were used and evaluated. Depending on the specific model selection, a very good agreement of the simulation data with the experimental results was achieved.

## 1. Introduction

To replace the highly toxic and carcinogenic hydrazine ( $N_2H_4$ ) for in-space propulsion, several so-called green propellants are under investigation. Among these green monopropellants are substances as ADN-based propellants, HAN-based propellants,  $H_2O_2$ , Water Propulsion systems (steam or as electrolytically decomposed hydrogen and oxygen) and nitrous oxide fuel blends. The named green propellants differ on many characteristics as e.g.  $I_{sp}$ , material compatibility, combustion temperature, ignitability, storability or cost. Thus, a single substance as replacement of hydrazine for all its applications is not in sight. Regarding the green alternatives, every advantage comes along with disadvantages, so research efforts have to be undertaken to solve all the corresponding challenges.

Since 2014, DLR conducts research on so-called "premixed monopropellants" consisting of nitrous oxide and hydrocarbons [1, 2, 3, 4, 5, 6, 7, 8]. These propellants are also called Nitrous Oxide Fuel Blends and investigated in different programs across the globe. So a first  $N_2O$ /fuel mixture consisting of  $N_2O$ ,  $C_2H_2$ ,  $C_2H_4$  and/or  $C_2H_6$  called NOFBX, was developed by the company Firestar [9, 10]. The NOFBX mixture seemed very promising, but to the authors knowledge it was too sensitive and exploded easily during test activities. Based on the NOFBX developments, a mixture of  $N_2O$  and  $C_2H_2$  named NA-7 was investigated by Boeing [11] which also resulted in explosions at the

NUMERICAL SIMULATIONS OF  $N_2O/C_2H_4$  COMBUSTOR AND COMPARISON TO EXPERIMENTAL DATA

test bench [12]. In Europe, a Nitrous Oxide/Ethanol mixture was investigated in the frame of a first ESA project "European Fuel Development". The mixture showed quite promising characteristics, but only three hot firings in a rocket combustor could be conducted to the overheating of the injection system [13, 14, 15]. At DLR a  $N_2O/C_2H_4$  and later on a  $N_2O/C_2H_6$  propellant was studied in premixed configuration. To avoid explosive decomposition during hot firings, great effort was taken to develop suitable flame arresters [2, 7, 6]. In addition, the sensitivity of a premixed  $N_2O/C_2H_6$  propellant to adiabatic compression, the thermal stability of the propellant, the material compatibility and the miscibility was investigated [16]. Regarding rocket combustors, the research activities center around analysis of the propellant performance, combustor and thruster design as well as cooling investigations.

DLR calls the propellants HyNOx (Hydrocarbons with Nitrous Oxide)-propellants and in parallel to the investigations of the premixed blends, the oxidizer and fuel are also used in conventional bipropellant systems. In parallel to the experimental work on HyNOx propellants, CFD simulations are used to gain insight into the combustion processes of the used research thrusters. To model the combustion process appropriately, reaction mechanisms for the combustion of  $N_2O/C_2H_4$  and  $N_2O/C_2H_6$  were developed by DLR's Institute of Combustion Technology [17, 18, 19, 8]. The mechanism for  $N_2O/C_2H_6$  is also capable of modelling the  $N_2O/C_2H_4$  combustion, this allows direct comparison of both mechanisms. The developed reaction mechanisms were used to design appropriate flame arresters for the monopropellant operation [2, 6], to derive laminar flame speeds and are finally used to simulate the whole combustion process inside the rocket combustor. By using the CFD simulations, insight in the combustion process should be gained. So e.g. the flame position, heat loads to the chamber walls or flow fields inside the chamber can be assessed. Furthermore, by using appropriate numerical setups, the geometrical sizing of the combustor or injection system can be improved. The research activities concerning HyNOx propellants are conducted in the frame of DLR's Future Fuels/NeoFuels project [8, 20] and in the frame of the ESA activity "High Performance Propellant Development" [16].

The present paper will give an overview of the numerical activities regarding the combustion of a premixed  $N_2O/C_2H_4$  propellant. The CFD-simulations were performed by using the commercial Software package Ansys Fluent and the mentioned reaction mechanisms developed by DLR's Institute of Combustion Technology. To assess the quality and capability of the conducted simulations, the resulting chamber pressure, thrust and heat flux were compared to the experimental data of a research thruster.

## 2. Test Bench and Experimental Setup

At the Institute of Space Propulsion of DLR in Lampoldshausen, the M11 test facility is available as flexible test platform for all kinds of advanced and green propellants [21, 22]. To perform the HyNOx tests, a dedicated test position is available. The test position is equipped with tanks, feeding lines, pressure regulators, valves, numerous sensors and a measurement and control system. Typically, different test specimens or thrusters are mounted in parallel and thus a quick replacement is possible.

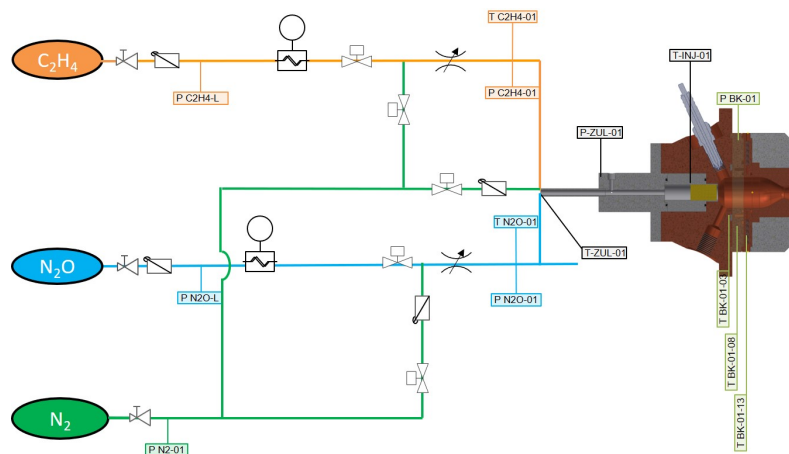


Figure 1: Simplified piping and instrumentation diagram of the test bench setup

Figure 1 shows the simplified piping and instrumentation diagram of the test setup. The propellant is fed from several 50 L gas bottles outside the test container, while the corresponding mass flow is adjusted via pressure regulators and control/regulating valves. In the feeding lines the mass flow is measured via coriolis mass flow meters and the propellant condition is assessed via temperature and pressure sensors in the corresponding feeding lines. The nitrous oxide and ethene lines as well as the thruster can be purged via nitrogen. Mixing of  $N_2O$  and  $C_2H_4$  or  $C_2H_6$  takes

NUMERICAL SIMULATIONS OF  $N_2O/C_2H_4$  COMBUSTOR AND COMPARISON TO EXPERIMENTAL DATA

place 0.5 m upstream the injector at a tube junction. Figure 1 also shows the instrumentation of the combustor which comprises of a chamber segments, equipped with temperature and pressure sensors. Ignition is achieved via spark plug.

## 2.1 Research Combustor

Figure 2 shows sectional views of the used research combustor (called TECHNO = Test Combustor for Hydrocarbons and Nitrous Oxide). The combustor consists of the propellant feeding system with a porous injector, a spark plug for ignition, temperature and pressure sensors, different chamber segments and a nozzle segment. All chamber parts are manufactures of CuCr1Zr, the combustor is not actively cooled and the copper parts act as heat sink (capacitively cooling).

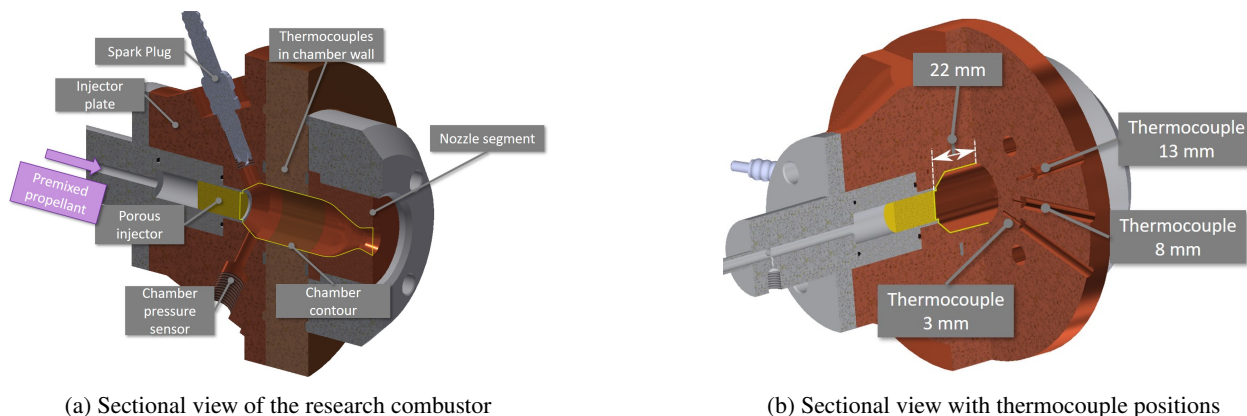


Figure 2: Sectional views of the used research combustor (named: TECHNO)

While 2a gives the main parts of the combustor, 2b shows the thermocouples' position which were used to determine the heat flux into the chamber walls. The thermocouples are placed in 22 mm axial distance from the injector head at three different radial positions from the inner chamber wall. The thermocouples' position in different depths allow the prediction of the heat flux via using an inverse method [23, 5]. The experimentally derived heat flux, the measured chamber pressure as well as the thrust were used to compare the test results to the CFD simulations. Table 1 gives the main geometrical parameters of the simulated combustor.

Research Combustor Parameter	Value
Length [mm]	60.5
Nozzle throat diameter [mm]	5
Chamber diameter [mm]	24
Characteristic chamber length $L^*$ [m]	1.02

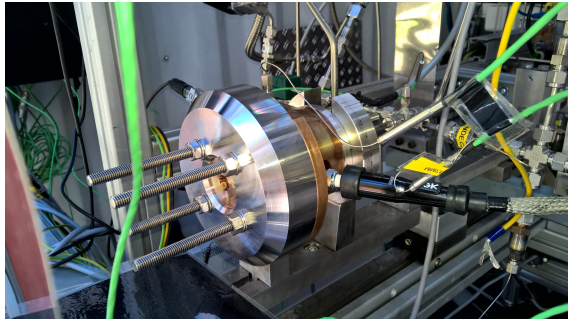
Table 1: Geometrical properties of the simulated and tested combustor

Figure 3a shows a side view of the research combustor mounted at DLR's M11.5 test bench in Lampoldshausen. The segmented design, the nozzle part, the spark plug for ignition, a thermocouple at the injector and the feeding lines can be seen. In addition, Figure 3b shows the combustor during hot firing.

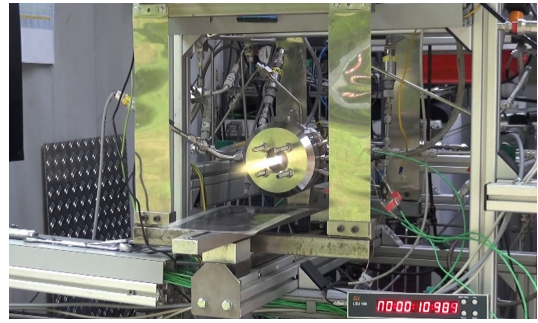
## 2.2 Test Procedure and Typical Test Data

Figure 4 shows a typical test sequence of a 10 s combustion test performed with the research combustor. At  $t = -13$  s the main valves open to pressurize the setup to the flow control valves. In addition, the nitrogen purge opens (compare Fig. 1). After three seconds of purging, the nitrogen valve closes again. At  $t = -0.25$  s the spark plug is activated and at  $t = 0$  s the flow control valves of  $N_2O$  and  $C_2H_6$  open. 0.5 s after opening of the flow control valves, the spark plug is deactivated. The flow control valves are closed at  $t = 10$  s, after additional 10 s of waiting time, the nitrogen purge is activated again. Finally, the automated test sequence stops 30 s after opening of the main valves.

Figure 5a shows the pressure data of a typical test run. After the initial nitrogen purging, the thruster is ignited at  $t = 0$  s. The orange and light blue line indicate the feeding pressure of ethene (P-C2H4-01) and nitrous oxide (P-N2O-01) upstream the porous injector. A pressure drop of approximately 12 bar across the injector is caused by

NUMERICAL SIMULATIONS OF  $N_2O/C_2H_4$  COMBUSTOR AND COMPARISON TO EXPERIMENTAL DATA

(a) Research combustor mounted at the test bench



(b) Combustor during hot firing

Figure 3: Combustor at the test bench M11.5 of DLR

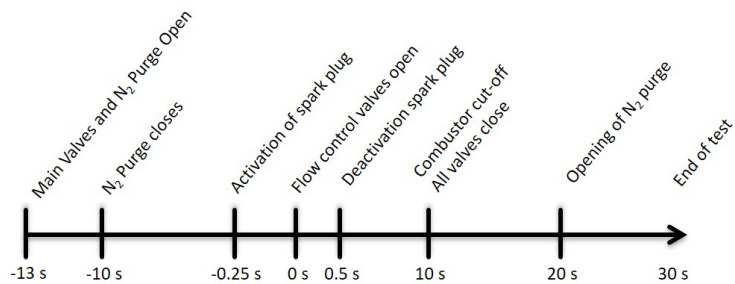
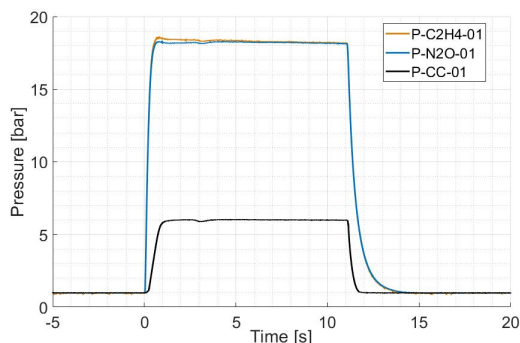


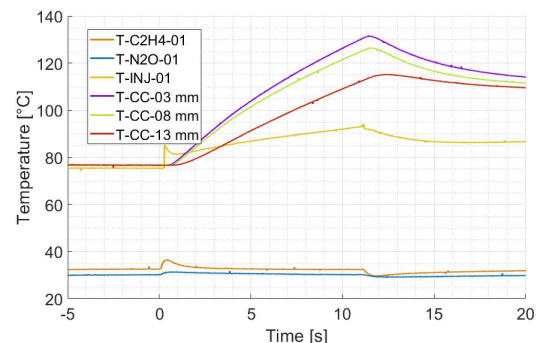
Figure 4: Typical test sequence

the fine structure and length of the porous material used during these tests. The high pressure drop causes a highly turbulent flow of  $N_2O$  and  $C_2H_4$  entering the combustor. During the shown test run, a chamber pressure (P-CC-01) of approximately 6 bar was reached.

Figure 5b gives the corresponding temperatures during the test run. Here T-CC-03 mm to T-CC-13 mm indicate the thermocouples at different radial distances from the inner chamber wall (compare Fig. 2b). T-Inj marks the injector head temperature as well as T-C<sub>2</sub>H<sub>4</sub> and T-N<sub>2</sub>O indicate the feeding temperatures of  $N_2O$  and  $C_2H_4$ .



(a) Pressure data of a typical test run



(b) Temperature data of the corresponding test run

Figure 5: Experimental data for pressure and temperature

### 2.3 Setup of the CFD Simulations and Boundary Conditions

The following section outlines the computational domain and boundary conditions as well as the general simulation setup.

### 2.3.1 Computational Domain

The numerical grid was created using Ansys ICEM 2020 R1. The two-dimensional mesh consists of about 78 000 cells for the combustion chamber. To reduce the computational effort, only one half of each combustion chamber was simulated, implying an axisymmetric boundary condition on the middle axis (yellow). A single inlet (red), wall (purple) and the nozzle exit (blue) complete the boundary of the mesh, as can be seen in Figure 6. The mesh close to the wall is refined to ensure a  $y^+$  value of  $\approx 1$ , which translates into an initial cell height of  $\approx 1 \mu m$ .

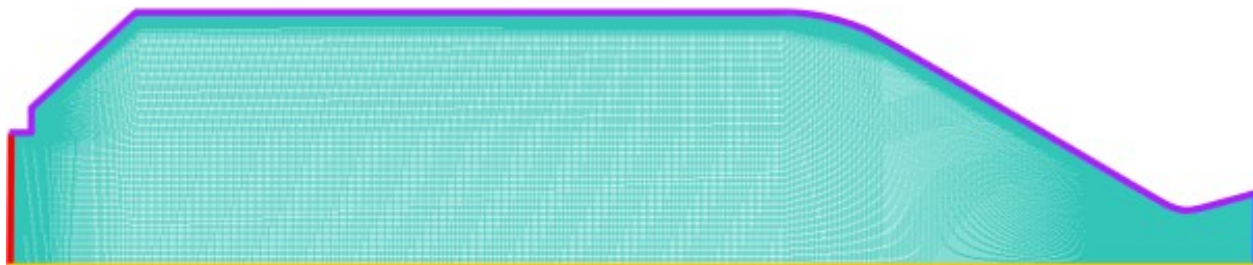


Figure 6: Computational grid of the first combustor

A convergence study was conducted for the combustion chamber with a coarse mesh (number of cells halved) and a finer meshes (number of cells doubled). To investigate the converging behaviour, the area-weighted average pressure and mass-weighted average temperature were observed. The finer mesh showed an unexpected deviation for the averaged pressure (see Figure 7), hence a fourth mesh with quadrupled number of cells was simulated. The results from this fourth mesh confirmed the original mesh, leading to the acceptance of the latter.

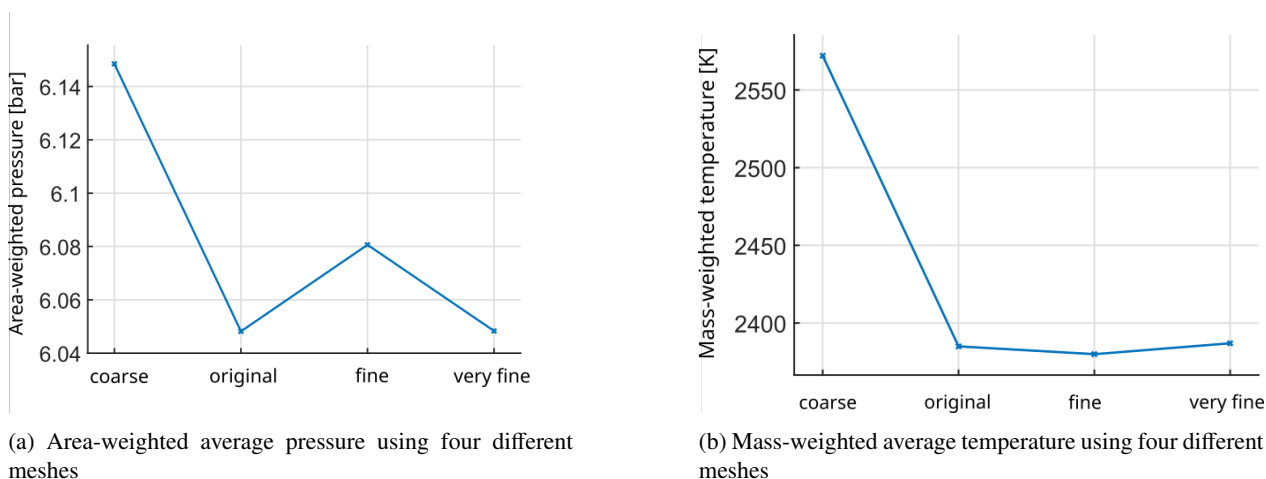


Figure 7: Convergence study using four different meshes

As can be seen in Figure 6, the propellant inlet is located on the left of the combustion chamber. A mass flow boundary condition is applied using the measured flow rate from the experiment at 300 K. The mass fractions of oxidizer and fuel was chosen according to the mixture ratio (ROF) of the respective experiment. Oxidizer and fuel are assumed to be perfectly mixed before entering the combustion chamber. An extensive study was conducted to identify the turbulence intensity at the inlet. As no information about the state of turbulence could be gained from experiments or found in the literature, multiple different values were investigated, ranging from 5% to 25%. For all walls, a no slip boundary condition with a fixed temperature value of 400 K was implemented. This represents the average temperature found at the wall during firing time (compare temperature data in Fig. 5b). The burnt propellant leaves the combustion chamber to the right of the computational domain and a pressure outlet boundary condition with ambient pressure is imposed.

### 2.3.2 Simulation Setup

For all simulations, the commercial CFD software Ansys Fluent 2020 R1 was used. The coupled pressure-based solver in axisymmetric, two-dimensional configuration was applied. Although stationary simulations were conducted,

NUMERICAL SIMULATIONS OF N<sub>2</sub>O/C<sub>2</sub>H<sub>4</sub> COMBUSTOR AND COMPARISON TO EXPERIMENTAL DATA

a transient state had to be considered for some simulations to achieve convergence. To calculate the flow field, the conservation equations for mass, energy and momentum in three spatial directions are employed.

$$\frac{\partial \rho}{\partial t} + \operatorname{div}(\rho \cdot \vec{v}) = 0 \quad (1)$$

$$\frac{\partial(\rho \vec{v})}{\partial t} + \operatorname{div}(\rho \cdot \vec{v} \otimes \vec{v}) - \operatorname{div}(\underline{\tau}) + \operatorname{grad}(p) = 0 \quad (2)$$

$$\frac{\partial(\rho \cdot E)}{\partial t} + \operatorname{div}(\rho \cdot \vec{v} \cdot E + p \cdot \vec{v} - \underline{\tau} \cdot \vec{v}) - \rho \cdot w_q = 0 \quad (3)$$

where  $\rho$  is the density,  $\vec{v}$  the velocity vector,  $p$  the pressure,  $E$  the total energy and  $w_q$  the specific heat source density.  $\underline{\tau}$  is the viscous stress tensor, containing shear and normal stresses. It can be described as

$$\underline{\tau} = \mu \left( \operatorname{div} \vec{v} + (\operatorname{div} \vec{v})^T \right) \quad (4)$$

Together with the thermal and caloric equation of state, all relevant quantities in the flow field can be calculated.

To account for turbulence, multiple RANS models were investigated, being the  $k$ - $\omega$  SST model, the standard, RNG and realizable  $k$ - $\epsilon$  model as well as the RSM model. Both the  $k$ - $\omega$  SST and the  $k$ - $\epsilon$  models close the Reynolds-averaged Navier-Stokes equations by applying the Boussinesq hypothesis and introducing two new variables:  $k$  as the averaged turbulent energy and  $\omega$  as the specific rate of dissipation or  $\epsilon$  as the dissipation of turbulent kinetic energy. In contrast, the RSM avoids the Boussinesq hypothesis and computes the viscous stress tensor directly, which in return has a negative impact on computational runtime [24].

Two species transport models were investigated in the present study: the Eddy-Dissipation-Concept (EDC) [25] and the Finite-Rate-Model (FRM) [26]. The EDC accounts for the interaction of turbulence with the chemical reactions, hence this model was initially chosen to model the combustion. Even though the FRM neglects the coupling of turbulence with chemical reactions, the model was selected as an alternative to the EDC within the scope of this work. Further information about the two models can be found in [26]. To converge the simulation, a first order upwind scheme was initially applied and subsequently switched to a second order upwind scheme. Different chemistry-solver were used for the two reaction mechanisms: For the N<sub>2</sub>O/C<sub>2</sub>H<sub>4</sub> reaction mechanism, the stiff-chemistry-solver was applied whereas for the N<sub>2</sub>O/C<sub>2</sub>H<sub>6</sub> reaction mechanism, the Chemkin-solver was used. Both chemistry solvers access an ISAT table, whereby the computational time of each iteration can be heavily reduced.

The simulation was initialized using the Hybrid Initialization in ANSYS Fluent. To start the combustion process, a small circular patch (6 mm diameter) was set to 3000 K for 10 iterations, imitating an igniter. This procedure was repeated 10 times to ensure that the flame does not extinguish during the ignition process.

## 2.4 Reaction Mechanisms and Combustion Modelling

To enable efficient CFD simulation, reduced chemical kinetic models were applied for the modeling of the reactions. The chemical kinetic model for the C<sub>2</sub>H<sub>4</sub> / N<sub>2</sub>O combustion was based on an updated version of the GRI 3.0 and was reduced to 22 species [1, 17]. For the modeling of the C<sub>2</sub>H<sub>6</sub> / N<sub>2</sub>O the C2 model DLR SynNG [27] was combined with the nitrogen submodel from Glarborg et al. [28]. In a second step this model was reduced to 35 species [29, 19].

For both models, the rapid reduction method of the linear transformation model (linTM) was applied [30, 31]. The linTM analyses species profiles and laminar flame speed profiles by means of characteristic points on the profiles. Examples for these characteristic points would be the coordinates of the curve maximum or the point where one third of the maximum is reached. Subsequently, the sensitivities of the  $x$  and  $y$  coordinates from the model parameters (e.g. Arrhenius coefficients) are determined with a brute-force approach. With the linTM, these information are used for sensitivity analyses (SA) of reaction systems and optimizations of chemical kinetic mechanisms.

The rapid reduction is achieved by the combination of the SA and the optimization capability of the linTM [30]. In a first step of the rapid reduction, species profiles and flame speed profiles are generated with a detailed chemical kinetic model for user given boundary conditions, e.g. engine conditions. With the SA important reactions are identified and reactions with a low sensitivity are removed from the mechanism, consequently reducing the numbers of species. Subsequently, the reduced model is post-optimised to achieve the same predictability of the initially created species profiles and flame speed profiles. This last step allows significantly smaller reduced mechanism compared to conventional methods without a post-optimization step [30].

Figure 8 exemplary compares the performance on the reproduction of laminar burning velocities for each post-optimized chemical kinetic model to the corresponding detailed models [1, 29, 19]. Here the burning velocity is plotted versus the equivalence ratio ( $\phi = \frac{ROF_{stoichiometric}}{ROF}$ ). The post-optimized model is in excellent agreement with this

NUMERICAL SIMULATIONS OF N<sub>2</sub>O/C<sub>2</sub>H<sub>4</sub> COMBUSTOR AND COMPARISON TO EXPERIMENTAL DATA

combustion characteristic, for which laminar burning velocities are an important indicator of an adequate heat release from the reactions.

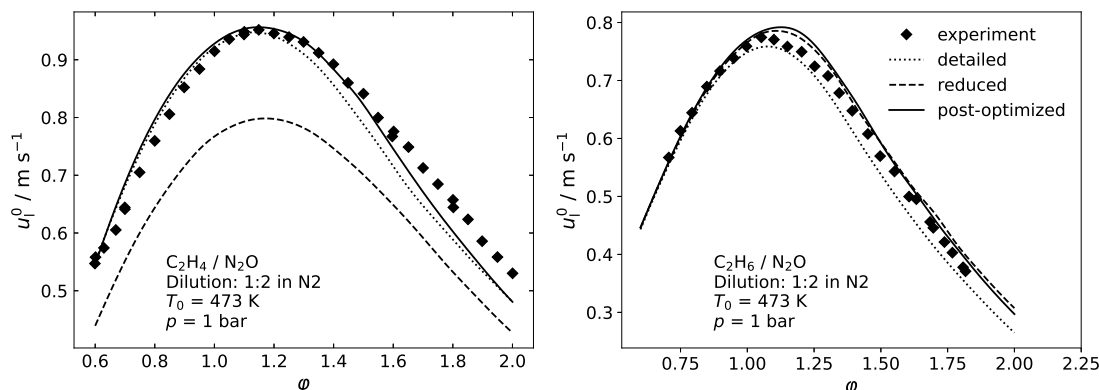


Figure 8: Laminar burning velocities with experimental data for C<sub>2</sub>H<sub>4</sub> [29] (left) and C<sub>2</sub>H<sub>6</sub> [17] (right), compared to the results of the corresponding detailed, reduced and post-optimized chemical kinetic model

### 3. Results of the CFD Simulations and Comparison to the Experiments

During the CFD study, multiple parameters as well as combustion and turbulence models were investigated to find the best performing simulation setup. In this chapter, these parameters are presented and their effect on the combustion is described. A single experiment (experimental data shown in Fig. 5a and Fig. 5b) was selected and reproduced with the following properties:

Table 2: Properties of investigated experiment

$ROF$ [-]	$\dot{m}$ [g/s]	$p_{exp}$ [bar]	$F_{exp}$ [N]
7.02	7.79	6.03	11.7

#### 3.1 Simulations by Using the Eddy Dissipation Concept (EDC)

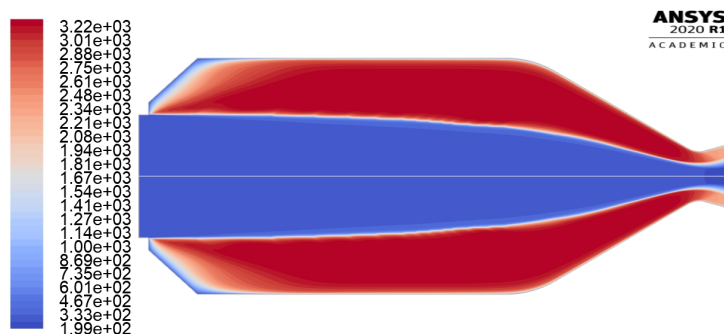
The EDC was initially chosen as the combustion model. To model turbulence, the  $k$ - $\omega$  SST model as well as the  $k$ - $\epsilon$  models and the RSM were applied. A summary of the Fluent case is given in Table 3.

Table 3: Summary of Fluent setup for the converged solution

Parameter	Setting
Combustion model	EDC
Solver	Coupled, pseudo transient ( $\Delta t = 1 \times 10^{-4}$ s)
Discretization method	Second-Order Upwind Scheme
Chemistry solver	Stiff-Chemistry Solver
Reaction mechanism	N <sub>2</sub> O/C <sub>2</sub> H <sub>4</sub>
Turbulence intensity	5%, 15%, 25%

In Figure 9, the temperature profile for the converged solution of the  $k$ - $\omega$  SST model is displayed. It can be observed, that a large part of the incoming propellant leaves the combustion chamber without combusting.

The difference between experimental pressure and simulated pressure was by far greater than 10%, hence the experiment could not be reproduced. Other turbulence models were applied, including three  $k$ - $\epsilon$  models as well as the RSM. The temperature profiles were similar to the one shown in Figure 9 and the combustion chamber pressure was consistently too small. As a consequence, the turbulence intensity was gradually increased from 5% to 15% and finally

NUMERICAL SIMULATIONS OF N<sub>2</sub>O/C<sub>2</sub>H<sub>4</sub> COMBUSTOR AND COMPARISON TO EXPERIMENTAL DATAFigure 9: Developed temperature profile in K (EDC and  $k-\omega$  SST model applied)

25% for the mentioned turbulence models. In all cases, an increase in pressure could be observed, although it never reached the experimental pressure within an acceptable range.

Based on [32], the model constants  $C_\gamma$  and  $C_\tau$  of the EDC were altered. Similarly, the turbulent Prandtl number and the turbulent Schmidt number were altered. A change in pressure was observed, but again never reached acceptable values close to the experimental pressure. This was also the case when implementing a radiation model. The Discrete Transfer Radiation Model [26] as well as the Discrete Ordinates model [33] were applied, both having a neglectable impact on the combustion.

To sum up, multiple simulations with the EDC were conducted, changing a wide range of parameters and models. It was not possible to reach a sufficiently high combustion chamber pressure and thus a sufficient agreement with the experimental data. As unburnt propellant left the combustor and thus the chamber pressure was low, the modelled combustion efficiency was also far below the experimental values.

### 3.2 Simulation by Using the Finite Rate Model (FRM)

As the EDC was not capable of reproducing the experiment, the FRM was applied. All other Fluent settings are consistent with Table 3. Again, the influence of the turbulence model and intensity were investigated. As the  $k-\omega$  SST and the standard  $k-\epsilon$  models were the most promising models, these two models were applied, each with 5%, 15% and 25% of turbulent intensity. The developed temperature profile is displayed in Figure 10.

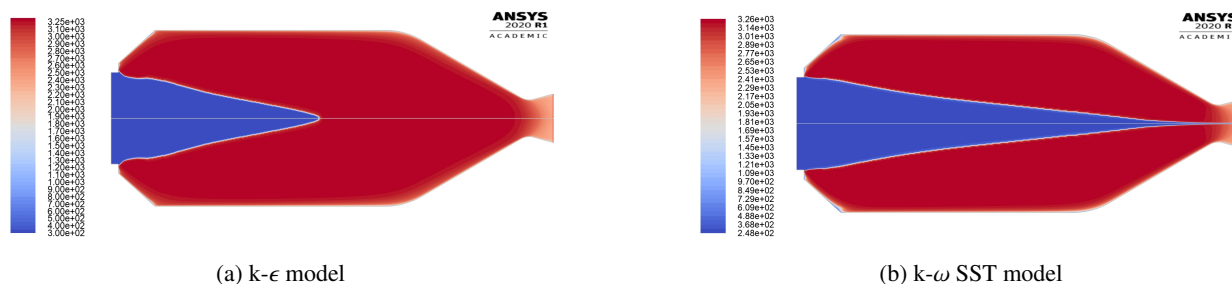


Figure 10: Temperature profiles in K, using FRM and 5% turbulence intensity

Comparing Figure 10 to Figure 9, the difference is clearly visible: for the FRM models, the entering propellant mixture combusts nearly completely. This is also represented by the combustion chamber pressure, which amounts to 6.12 bar for the  $k-\epsilon$  model and to 6.15 bar for the  $k-\omega$  SST model. In this case, changing the turbulence intensity to 25% only had a small impact on the simulation results. For increasing the turbulence intensity while using the  $k-\omega$  SST model, the pressure dropped to 6.15 bar. In contrast, changing the turbulence intensity for the  $k-\epsilon$  model, resulted in an unchanged pressure. To compare the simulated thrust with the measured thrust equation 5 is used:

$$F = \dot{m}v_e + (p_e - p_a)A_e \quad (5)$$

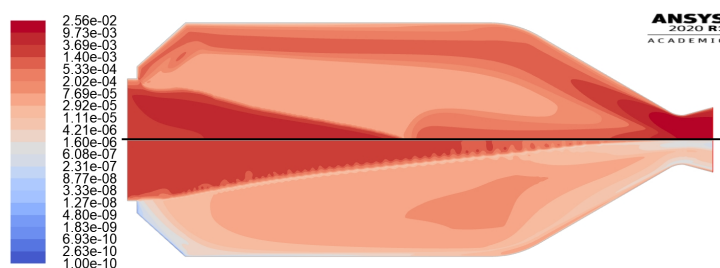
where  $\dot{m}$  is the mass flow rate given as boundary condition,  $A_e$  indicates the exit area of the nozzle and  $p_a$  the ambient pressure.  $v_e$  and  $p_e$  are extracted from the simulation as mass-weighted average velocity and area-weighted average pressure at the nozzle exit.

NUMERICAL SIMULATIONS OF N<sub>2</sub>O/C<sub>2</sub>H<sub>4</sub> COMBUSTOR AND COMPARISON TO EXPERIMENTAL DATA

Table 4: Results of simulation using the FRM

Turbulence model	Turbulence intensity	$p_c$ [bar]	$F_c$ [N]
k- $\omega$ SST	5%	6.16	13.5
	15%	6.16	13.5
	25%	6.15	13.5
k- $\epsilon$	5%	6.12	13.3
	15%	6.12	13.3
	25%	6.12	13.3
Experiment		6.03	11.71

A summary of the simulation results is given in Table 4. The k- $\epsilon$  SST model tends to better capture the flow physics. The reason for the shorter flame as well as the lower combustion chamber pressure for the k- $\epsilon$  model stems from a higher production of turbulent viscosity.

Figure 11: Contour of turbulent viscosity with the k- $\epsilon$  model (upper half) and the k- $\omega$  SST model (lower half)

As Figure 11 reveals, the turbulent viscosity is greater for the k- $\epsilon$  model than for the k- $\omega$  SST model. This leads to a higher dissipation of turbulent kinetic energy, hence the shorter flame. It also influences the combustion chamber pressure, as more heat is lost to the chamber wall, reducing the energy content in the combustion chamber. These findings are in accordance with [34].

### 3.2.1 Wall Heat Flux

To investigate the experimental heat flux, an inverse method was applied to the temperature data, measured in the combustion chamber wall. Based on [35], an iterative procedure was implemented, which is capable of calculating the wall heat flux at each time step during the experiments. The hereby approximated wall heat flux for the experiment described in Table 2 amounts to 1010 kW/m<sup>2</sup>.

Table 5: Heat flux comparison between experiment and simulation

Turbulence model	Turbulence intensity	$\dot{q}$ [kW/m <sup>2</sup> ]
k- $\omega$ SST	5%	720
	15%	790
	25%	836
k- $\epsilon$	5%	909
	15%	910
	25%	920
Experiment		1010

Table 5 gives an overview of the simulated heat flux. Together with Table 4, it clearly shows that the k- $\epsilon$  model with a turbulence intensity of 25% represents the experiment with very low deviations.

### 3.3 Simulated Experiments

In the previous sections, different parameters and models were investigated for a single experiment (compare Fig. 5a and 5b). As a result, the FRM in combination with the k- $\epsilon$  model and 25% turbulence intensity was identified to

NUMERICAL SIMULATIONS OF  $N_2O/C_2H_4$  COMBUSTOR AND COMPARISON TO EXPERIMENTAL DATA

best capture the flow physics in the combustion chamber. Hence, these models and model parameters were selected to reproduce further experiments. A wide range of operating points were selected to validate the applied simulation setup. The combustion pressure and the thrust were easily comparable with the experimental value, though this was not the case for the wall heat flux. Due to a high axial heat flux, the thermocouple did not exclusively capture the heat flux coming from the combustion chamber, but also from the nozzle segment (compare Fig. 2. Depending on the operating point, a very high nozzle heat flux could eventually have a great impact on the measured temperature data. As no thermocouples were placed within the nozzle, it was not possible to approximate the nozzle heat flux and hence the wall heat flux could not be satisfactorily calculated. The following table gives an overview of the simulated experiments, together with the measured data:

Table 6: Summary of simulated experiments

No. experiment	$ROF$	$\dot{m}[g/s]$	$p_{exp}$ [bar]	$p_{sim}$ [bar]	$F_{exp}$ [N]	$F_{sim}$ [N]	$\dot{q}_{exp}$ [kW/m <sup>2</sup> ]	$\dot{q}_{sim}$ [kW/m <sup>2</sup> ]
0	7.02	7.79	6.03	6.12	11.7	13.3	1010	920
1	7.03	4.51	3.41	3.48	5.6	6.0	620	654
2	6.99	11.98	9.54	9.54	20.1	22.7	*	1189
3	10.4	10.07	7.58	7.63	15.4	17.5	*	1075
5	7.34	3.53	2.64	2.6	3.9	3.82	520	577
6	7.31	9.48	7.37	7.39	15.0	16.9	950	1037

\* Calculation of experimental heat flux not possible

Table 6 indicates, that with the determined models, all operating points can be excellently reproduced. Considering that the combustion chamber pressure is the most reliable comparison parameter, its deviation does not exceed 1.5%. This is well within the experimental measurement errors and thus regarded as high precision result. The deviations in thrust are higher, but due to the experimental setup, here the experimental error has to be considered in the range of  $\pm 1.5$  N. In cases where the heat flux could be calculated, the deviation remains below 12%.

### 3.4 Simulation with the $N_2O/C_2H_6$ Reaction Mechanism

The simulation setup was not only transferred to different operating points, but also the  $N_2O/C_2H_6$  mechanism was used. As already mentioned, this mechanism is capable of modelling the combustion of both  $C_2H_6$  and  $C_2H_4$ . Therefore, the experiment introduced in Table 2 was simulated using the  $N_2O/C_2H_6$  mechanism as well. The chemistry solver had to be switched to the Chemkin solver to read in the mechanism. Applying the same setup as with the previously used mechanism, it was not possible to achieve convergence. Only by switching to a transient solver, it was possible to balance out the energy that was entering and leaving the computational domain and achieve energy conservation. Upon changing to the transient solver, the residuals eventually dropped to an acceptable level of  $\approx 10^{-4}$ . To approximate the required time step size, the flame thickness for each species  $k$  was divided by the laminar flame velocity  $S_L$ . As a result, a transient time step size  $\Delta t = 5 \times 10^{-5}$ s was determined. A summary of the simulation setup can be found in Table 7:

Table 7: Summary of Fluent setup for the  $N_2O/C_2H_6$  mechanism

Parameter	Setting
Combustion model	FRM
Solver	Coupled, transient ( $\Delta t = 5 \times 10^{-5}$ s)
Discretization method	Second-Order Upwind Scheme
Chemistry solver	Chemkin solver
Reaction mechanism	$N_2O/C_2H_6$
Turbulence intensity	15%

The converged solution can be compared with the solution of the  $N_2O/C_2H_4$  mechanism. As table 7 shows, the combustion chamber pressure tends to be better captured by the  $N_2O/C_2H_6$  mechanism, whereas the simulated wall heat flux differs greater from the experimental heat flux. There is only a slight difference in the simulated thrust.

NUMERICAL SIMULATIONS OF N<sub>2</sub>O/C<sub>2</sub>H<sub>4</sub> COMBUSTOR AND COMPARISON TO EXPERIMENTAL DATA

Table 8: Comparison of different mechanisms and the measured data

Mechanism	$p$ [bar]	$F$ [N]	$\dot{q}$ [kW/m <sup>2</sup> ]
N <sub>2</sub> O/C <sub>2</sub> H <sub>4</sub>	6.12	13.3	920
N <sub>2</sub> O/C <sub>2</sub> H <sub>6</sub>	6.03	13.2	1177
Experiment	6.02	11.7	1010

### 3.5 Discussion and Lessons Learnt

The differences between experimental and simulated results are manifold and explained in this chapter. The simulated pressure was within the measurement uncertainty, yielding good agreement with the experiments. The simulated thrust, which in most cases had a greater discrepancy but never exceeded 2 N, was calculated assuming an ideal nozzle (compare Equation 5). In general, this assumption does not hold for a real thruster. Also the experimental thrust measuring device itself bears uncertainties. In addition, mountings, pipes and other components are heated up during the hot gas tests and thereby move, which falsifies the measurement of the thrust. The wall heat flux as the third comparison parameter can be accurately extracted from the simulation. Although the applied inverse method worked well, it cannot reproduce the exact wall heat flux. The thermocouples itself feature uncertainties as well as their positioning in the experiments might not be perfect. The present study also demonstrated, that the nozzle heat flux can have a very high impact on the thermal distribution in the combustion chamber wall. As only a limited amount of thermocouples were installed, a precise approximation of all combustion chamber heat fluxes is not possible. Given that the calculated experimental heat fluxes are hard to predict, the inverse method still provides good agreement with the simulated heat fluxes.

The following section shall give some hints about how to get reproducible results from a CFD simulation for the used N<sub>2</sub>O/C<sub>2</sub>H<sub>4</sub> or N<sub>2</sub>O/C<sub>2</sub>H<sub>6</sub> mechanisms in a rocket combustor:

- The N<sub>2</sub>O/C<sub>2</sub>H<sub>6</sub> mechanism requires substantially more patching iterations, otherwise the flame extinguishes. Instead of patching for 10 times every 10 iterations, it required around 40 times every 10 iterations to sustain the flame. Also the patching temperature was increased to 3500 K.
- Starting with a First-Order discretization scheme for a couple of hundreds iterations and then switching to a Second-Order discretization after the residuals do not change anymore helps in achieving convergence.
- When interrupting the solution procedure and closing Ansys Fluent, it is important to save the ISAT table in a separate file. When the simulation is restarted, the ISAT table can be read again. As the ISAT table is saved in the RAM, restarting the simulation without loading the ISAT table will result in a sharp increase in residuals which in return takes a substantial amount of time to resume to the previous level. It can also be helpful to increase the maximum storage memory of the ISAT table.
- Not using the ISAT table results in an immense increase in computational time and turned out to be inevitable.
- If problems occur when loading the reaction mechanism, make sure to select the correct chemistry solver. Ansys Fluent has a threshold for some values given in the mechanism file. Unfortunately, no error message appears when these thresholds are exceeded. The thresholds are:
  - ⇒  $-1 \times 10^{20} - 1 \times 10^{38}$  for the Pre-Exponential Factor
  - ⇒  $-1 \times 10^{20} - 1 \times 10^{38}$  for the Activation Energy
  - ⇒  $-1 \times 10^{20} - 1 \times 10^{20}$  for the Temperature Exponent

The actual values can either be checked in the mechanism file itself or in Fluent under **Models** → **Species** → **Edit** in the field *Mixture Properties* → **Edit** in the field *Reaction*.

## 4. Summary and Outlook

N<sub>2</sub>O/C<sub>2</sub>H<sub>6</sub> and N<sub>2</sub>O/C<sub>2</sub>H<sub>4</sub> are promising propellant combinations for in-space propulsion. In the present paper, the combustion inside a research thruster using these propellants was investigated with the commercial CFD software Ansys Fluent. The aim was to reproduce previously conducted experiments and therefore get an insight into the combustion processes. To model the combustion, two reaction mechanisms were developed by DLR's Institute of Combustion Technology, which were both used within the scope of this paper. The initially used mechanism is capable

NUMERICAL SIMULATIONS OF N<sub>2</sub>O/C<sub>2</sub>H<sub>4</sub> COMBUSTOR AND COMPARISON TO EXPERIMENTAL DATA

of modelling the combustion of N<sub>2</sub>O with C<sub>2</sub>H<sub>6</sub> whereas the second mechanism can model the combustion of N<sub>2</sub>O with both hydrocarbons, C<sub>2</sub>H<sub>6</sub> and C<sub>2</sub>H<sub>4</sub>. To compare the simulations with the experiments, the combustion chamber pressure, the thrust and the wall heat flux were examined. As the pressure was directly measured in the combustion chamber, it represents the most reliable comparison parameter. Several numerical parameters and models were applied to determine the best simulation setup. So the Eddy Dissipation Concept and the Finite Rate Model were evaluated regarding their ability to reproduce the experimental results. Furthermore, different turbulence models as the Reynolds-Stress Model (RSM), the k- $\epsilon$  and k- $\omega$  SST model were evaluated in combination with the corresponding reaction model. Finally transient and steady state simulations were conducted. It turned out that the Finite Rate Model (FRM) in combination with the k- $\epsilon$  model and a turbulence intensity of 25% at the inlet provided the best results. This setup was able to reproduce all investigated experiments with good accuracy. The simulated pressure always lay within the measurement uncertainty. The deviation in thrust was slightly larger, which could be addressed to the measurement uncertainty as well as to the assumptions of the ideal thrust equation. An inverse method was applied to the temperature data in order to retrieve the experimental heat flux. Even though the method is limited in terms of complexity due to a sparse number of thermocouples, it was able to reproduce the simulated heat flux with a deviation of less than 12%, as long as the axial heat flux remained nondominant. The findings were transferred to the second reaction mechanism (N<sub>2</sub>O/C<sub>2</sub>H<sub>6</sub>). It turned out that this mechanism requires a transient solver to converge. With this second mechanism, the gained results for the combustion chamber pressure were closer to the experimental pressure whereas the heat flux had a larger discrepancy.

In a next step, the reaction of premixed N<sub>2</sub>O/C<sub>2</sub>H<sub>6</sub> will be simulated and compared to experimental data. In parallel to the experiments with premixed HyNO<sub>x</sub>, also experiments with conventional bipropellants are conducted. Thus, in a further step the combustion of the HyNO<sub>x</sub> bipropellant in a research thruster will be simulated and evaluated.

## 5. Acknowledgments

The authors would like to thank DLR's M11 test bench team for their assistance in conducting the experiments. Further thanks go to Florian Merz for reviewing the paper.

## References

- [1] L. K. Werling, T. Hörger, K. Manassis, D. Grimmeisen, M. Wilhelm, C. Erdmann, H. K. Ciezki, S. Schleichriem, S. Richter, T. Methling, E. Goos, C. Janzer, C. Naumann, U. Riedel, Nitrous Oxide Fuels Blends: Research on Premixed Monopropellants at the German Aerospace Center (DLR) since 2014, in: AIAA Propulsion and Energy Forum and Exposition, 2020. AIAA Propulsion and Energy Forum 24.-26.08.2020, 24.-26.08.2020. doi:10.2514/6.2020-3807.
- [2] Lukas Werling, Entwicklung und Erprobung von Flammensperren für einen vorgemischten, grünen Raketentreibstoff aus Lachgas (N<sub>2</sub>O) und Ethen (C<sub>2</sub>H<sub>4</sub>): DLR-Forschungsbericht. DLR-FB-2020-39, 330 S, Dissertation, University of Stuttgart, Stuttgart (2020).
- [3] L. Werling, T. Hörger, Experimental analysis of the heat fluxes during combustion of a N<sub>2</sub>O/C<sub>2</sub>H<sub>4</sub> premixed green propellant in a research rocket combustor, *Acta Astronautica* 189 (2021) 437–451. doi:10.1016/j.actaastro.2021.07.011.
- [4] L. Werling, P. Bätz, Parameters Influencing the Characteristic Exhaust Velocity of a Nitrous Oxide/Ethene Green Propellant, *Journal of Propulsion and Power* 38 (2) (2022) 254–266. doi:10.2514/1.B38349.
- [5] N. Perakis, L. Werling, H. Ciezki, S. Schleichriem, Numerical Calculation of Heat Flux Profiles in a N<sub>2</sub>O/C<sub>2</sub>H<sub>4</sub> Premixed Green Propellant Combustor using an Inverse Heat Conduction Method, in: *Space Propulsion Conference*, 1.-5. May 2016, Rome, Italy.
- [6] L. Werling, F. Lauck, D. Freudenmann, N. Röcke, H. Ciezki, S. Schleichriem, Experimental Investigation of the Flame Propagation and Flashback Behavior of a Green Propellant Consisting of N<sub>2</sub>O and C<sub>2</sub>H<sub>4</sub>, *Journal of Energy and Power Engineering* 11 (12) (2017) 735–752. doi:10.17265/1934-8975/2017.12.001.
- [7] L. Werling, Y. Jooß, M. Wenzel, H. K. Ciezki, S. Schleichriem, A premixed green propellant consisting of N<sub>2</sub>O and C<sub>2</sub>H<sub>4</sub>: Experimental analysis of quenching diameters to design flashback arresters, *International Journal of Energetic Materials and Chemical Propulsion* 17 (3) (2018) 241–262. doi:10.1615/IntJEnergeticMaterialsChemProp.2019027950.

NUMERICAL SIMULATIONS OF N<sub>2</sub>O/C<sub>2</sub>H<sub>4</sub> COMBUSTOR AND COMPARISON TO EXPERIMENTAL DATA

- [8] T. Pregger, G. Schiller, F. Cebulla, R.-U. Dietrich, S. Maier, A. Thess, A. Lischke, N. Monnerie, C. Sattler, P. Le Clercq, B. Rauch, M. Köhler, M. Severin, P. Kutne, C. Voigt, H. Schlager, S. Ehrenberger, M. Feinauer, L. Werling, V. P. Zhukov, C. Kirchberger, H. K. Ciezki, F. Linke, T. Methling, U. Riedel, M. Aigner, Future Fuels—Analyses of the Future Prospects of Renewable Synthetic Fuels, *Energies* 13 (1) (2020) 138. doi:10.3390/en13010138.
- [9] M. Gregory, M. Vozoff, B. Rishikof, NOFBX: A new-nontoxic Green propulsion technology with high performance and low cost, in: 63rd International Astronautical Congress, 1-5 October 2012, Naples, Italy, 2012.
- [10] G. Mungas, NOFBX™ Propulsion Overview: Propulsion Challenges for Commercial Reusable Space Vehicles, in: 49th AIAA/ASME/SAE/ASEE Joint Propulsion Conference, 15. - 17. July, 2013, San Jose, California, USA, American Institute of Aeronautics and Astronautics, Reston, Virginia, 2013. doi:10.13140/RG.2.1.2032.1685.
- [11] T. Master, Airborne Launch Assist Space Access (ALASA).  
URL <https://www.darpa.mil/program/airborne-launch-assist-space-access>
- [12] Spacenews.com, DARPA Scraps Plan To Launch Small Sats from F-15 Fighter Jet (30.11.2015).  
URL <http://spacenews.com/darpa-airborne-launcher-effort-falters/>
- [13] A. E. Mayer, I. Waugh, M. Poucet, European Fuel Blend, Final Report: ESTEC Contract Number 4000113544/15/NL/AD.  
URL <https://artes.esa.int/projects/european-fuel-blend-development>
- [14] A. E. Mayer, W. Wieling, A. Watts, M. Poucet, I. Waugh, J. Macfarlane, F. Valencia-Bel, European Fuel Blend development for in-space propulsion, in: Space Propulsion Conference 14.-18.05.2018, Sevilla, Spain.
- [15] I. Waugh, E. Moore, J. Macfarlane, A. Watts, A. E. Mayer, Testing of a novel nitrous-oxide and ethanol fuel blend, in: Space Propulsion Conference 14.-18.05.2018, Sevilla, Spain.
- [16] L. Werling, M. Negri, F. Lauck, E. Goos, J. Wischek, Y. Besel, F. Valencia-Bel, High Performance Propellant Development - Overview of Development Activities Regarding Premixed, Green N<sub>2</sub>O/C<sub>2</sub>H<sub>6</sub> Monopropellants, in: 8th Space Propulsion Conference 2022, 09-13. May 2022, Estoril, Portugal, Vol. ID93.
- [17] C. Naumann, T. Kick, T. Methling, M. Braun-Unkhoff, U. Riedel, Ethene/nitrous oxide mixtures as green propellant to substitute hydrazine: Reaction mechanism validation, *International Journal of Energetic Materials and Chemical Propulsion* 19 (1) (2020) 65–71. doi:10.1615/IntJEnergeticMaterialsChemProp.2020028133.
- [18] C. Naumann, C. Janzer, U. Riedel, Ethane / Nitrous Oxide Mixtures as a Green Propellant to Substitute Hydrazine: Validation of Reaction Mechanism, in: 9th European Combustion Meeting (ECM), 14.-17.04.2019, Lisbon, Portugal.
- [19] C. Janzer, S. Richter, C. Naumann, T. Methling, “Green propellants” as a hydrazine substitute: experimental investigations of ethane/ethene-nitrous oxide mixtures and validation of detailed reaction mechanism, *CEAS Space Journal* 14 (1) (2022) 151–159. doi:10.1007/s12567-021-00370-8.
- [20] H. K. Ciezki, V. Zhukov, L. Werling, C. Kirchberger, C. Naumann, M. Friess, U. Riedel, Advanced Propellants for Space Propulsion - A Task within the DLR Interdisciplinary Project "Future Fuels", in: 8th European Conference for Aeronautics and Space Sciences (EUCASS), 1.-4. July 2019, Madrid, Spain. doi:10.13009/EUCASS2019-276.  
URL <http://www.eucass2019.eu/>
- [21] M. Wilhelm, L. Werling, F. Strauss, F. Lauck, C. Kirchberger, H. Ciezki, S. Schlechtriem, Test complex M11: Research on Future Orbital Propulsion Systems and Scramjet engines, in: 70th International Astronautical Congress, Washington, USA, 2019, Vol. IAC-19,C4,9,1,x49899.
- [22] H. K. Ciezki, L. Werling, M. Negri, F. Strauss, M. Kobald, C. Kirchberger, D. Freudenmann, M. Wilhelm, A. Petrarolo, 50 Years of Test Complex M11 in Lampoldshausen - Research on Space Propulsion Systems for Tomorrow, in: 7th European Conference for Aeronautics and Space Sciences (EUCASS), 03. - 06. Jul. 2017, Milano, Italy, 2017.  
URL <https://elib.dlr.de/117501/>
- [23] N. Perakis, O. J. Haidn, Inverse heat transfer method applied to capacitively cooled rocket thrust chambers, *International Journal of Heat and Mass Transfer* 131 (2019) 150–166. doi:10.1016/j.ijheatmasstransfer.2018.11.048.

NUMERICAL SIMULATIONS OF N<sub>2</sub>O/C<sub>2</sub>H<sub>4</sub> COMBUSTOR AND COMPARISON TO EXPERIMENTAL DATA

- [24] H. Oertel, *Strömungsmechanik*, Springer Verlag, 2015.
- [25] B. F. Magnussen, On the structure of turbulence and a generalized eddy dissipation concept for chemical reaction in turbulent flow, AIAA, Missouri, USA (1981).
- [26] Ansys, *Fluent Theory Guide*, Release 17.2, Help System.
- [27] T. Methling, M. Braun-Unkhoff, U. Riedel, An optimised chemical kinetic model for the combustion of fuel mixtures of syngas and natural gas, *Fuel* 262 (2020) 116611. doi:10.1016/j.fuel.2019.116611.
- [28] P. Glarborg, J. A. Miller, B. Ruscic, S. J. Klippenstein, Modeling nitrogen chemistry in combustion, *Progress in Energy and Combustion Science* 67 (2018) 31–68. doi:10.1016/j.pecs.2018.01.002.
- [29] C. Janzer, T. Methling, Ethane / nitrous oxide mixtures as green propellants substituting hydrazine: reduction of optimized reaction mechanism for CFD simulations, in: *Proc. 10th European Combustion Meeting (ECM)*, no. Paper 16, 2021, 14.-15.04.2021.
- [30] T. Methling, M. Braun-Unkhoff, U. Riedel, A novel linear transformation model for the analysis and optimisation of chemical kinetics, *Combustion Theory and Modelling* 21 (3) (2017) 503–528. doi:10.1080/13647830.2016.1251616.
- [31] T. Methling, *Entwicklung des linearen Transformationsmodells für die Analyse und Optimierung chemisch-kinetischer Prozesse*: Dissertation. doi:10.18419/opus-9430.
- [32] I. S. Ertesvag, Analysis of some recently proposed modifications to the eddy dissipation concept (edc), *Combustion Science and Technology* (2018). doi:10.1080/00102202.2019.1611565.
- [33] G. D. Raithby, E. H. Chui, A finite-volume method for predicting a radiant heat transfer in enclosures with participating media, *Journal of Heat Transfer (Transactions of the ASME (American Society of Mechanical Engineers), Series C); (United States)* 112:2 (5 1990). doi:10.1115/1.2910394.  
URL <https://www.osti.gov/biblio/5899181>
- [34] C. Roth, N. Perakis, O. J. Haidn, Modeling Combustion and Heat Transfer in a Single-Element GCH<sub>4</sub>/GOX Rocket Combustor, in: *Proceedings of the 7th International Conference on Fluid Flow, Heat and Mass Transfer (FFHMT'20)*, Vol. Paper No. 178, 2020. doi:10.11159/ffhmt20.178.
- [35] N. Perakis, O. J. Haidn, Inverse heat transfer method applied to capacitively cooled rocket thrustchambers, *International Journal of Heat and Mass Transfer* 131 (2019) 150–166 (2019). doi:<https://doi.org/10.1016/j.ijheatmasstransfer.2018.11.048>.